doi: 10.17586/2226-1494-2025-25-3-554-564

Automatic calibration of the receiving line of information and control systems in real time

Nguyen Trong Nhan[1]✉, Xuan Luong Nguyen[2], Phung Bao Nguyen[3]

[1] Air Defense - Air Force Technical Institute, Hanoi, 11400, Vietnam
[2] VNU University of Science, Hanoi, 100000, Vietnam
[3] Le Quy Don Technical University, Hanoi, 11917, Vietnam

[1] 10th20th30th@gmail.com✉, https://orcid.org/0000-0001-6626-893X
[2] nguyenxuanluong_sdh22@hus.edu.vn, https://orcid.org/0009-0000-6988-4738
[3] nguyenphungbao@lqdtu.edu.vn

Abstract
In this paper, the novel methodology for real-time automatic calibration of digital transceiver modules in the receiving path of information and control systems is presented. This methodology is grounded in the formation of calibration coefficients through a comparison between the complex signal amplitude at the output of the receiving path of the "virtual" reference module and the complex signal amplitude at the output of the receiving path following signal accumulation. The calibration value for each receiving path output complex signal amplitude is determined by multiplying the output complex signal amplitude by its corresponding calibration coefficient. The gain pattern of the information and control system is synthesized by calculating the weighted sum of the calibrated output complex signal amplitudes across all receiving paths, thereby maximizing the peak gain and minimizing side lobe levels. Simulations and experimental analyses were performed on an information and control system operating in the L-band to validate the proposed methodology. The results indicated a reduction in amplitude errors to 3.79 dB and a decrease in phase errors to 5°40′12″. The proposed methodology meets the requirements for synthesizing a self-calibrating subsystem model employing a soft configuration approach.

Keywords
information and control system, radiation pattern, gain pattern, reference module, calibration coefficient

For citation: Nhan N.T., Nguyen X.L., Nguyen P.B. Automatic calibration of the receiving line of information and control systems in real time. *Scientific and Technical Journal of Information Technologies, Mechanics and Optics*, 2025, vol. 25, no. 3, pp. 554–564. doi: 10.17586/2226-1494-2025-25-3-554-564

УДК 004.85

Автоматическая калибровка приемного тракта информационно-управляющих систем в режиме реального времени

Нгуен Чонг Нхан[1]✉, Суан Льюнг Нгуен[2], Фунг Бао Нгуен[3]

[1] Технический институт ПВО, Ханой, 11400, Вьетнам
[2] Ханойский государственный университет, Ханой, 100000, Вьетнам
[3] Вьетнамский государственный технический университет имени Ле Куй Дона, Ханой, 11917, Вьетнам

[1] 10th20th30th@gmail.com✉, https://orcid.org/0000-0001-6626-893X
[2] nguyenxuanluong_sdh22@hus.edu.vn, https://orcid.org/0009-0000-6988-4738
[3] nguyenphungbao@lqdtu.edu.vn

Аннотация
Введение. Представлена новая методика автоматической калибровки приемного тракта цифровых приемопередающих модулей в реальном времени. **Метод.** Методика калибровки основана на формировании калибровочных коэффициентов путем сравнения комплексной амплитуды сигнала на выходе приемного тракта «виртуального» эталонного модуля и комплексной амплитуды сигнала на выходе приемного тракта

после накопления сигнала. Калибровочное значение амплитуды комплексного сигнала на выходе каждого приемного тракта определяется с помощью умножения амплитуды комплексного сигнала на соответствующий калибровочный коэффициент. Диаграмма усиления информационно-управляющей системы синтезируется путем вычисления взвешенной суммы калиброванных амплитуд выходных комплексных сигналов по всем приемным трактам, что позволяет максимизировать пиковое усиление и минимизировать уровень боковых лепестков. **Основные результаты.** Для проверки предложенной методики проведены моделирование и экспериментальный анализ информационно-управляющей системы, работающей в L-диапазоне. Результаты показали снижение амплитудных ошибок до 3,79 дБ и фазовых ошибок до 5°40′12″. **Обсуждение.** Предложенная методика удовлетворяет требованиям к синтезу самокалибрующейся модели подсистемы с использованием подхода мягкой конфигурации.

Ключевые слова
информационно-управляющая система, диаграмма направленности излучения, коэффициент усиления, опорный модуль, калибровочный коэффициент

Ссылка для цитирования: Нхан Ч.Н., Нгуен С.Л., Нгуен Ф.Б. Автоматическая калибровка приемного тракта информационно-управляющих систем в режиме реального времени // Научно-технический вестник информационных технологий, механики и оптики. 2025. Т. 25, № 3. С. 554–564 (на англ. яз.). doi: 10.17586/2226-1494-2025-25-3-554-564

Introduction

In the current phase of technological development in multifunctional radar sensor systems, the proportion of Information and Control System (ICS) has grown significantly relative to conventional antenna types [1]. This expansion is driven by the need to achieve superior technical performance in such systems. ICS are composed of numerous transceiver modules which typically consist of functional units designed and manufactured using various active and passive components. Over time, due to factors, such as manufacturing variability, temperature fluctuations, aging, and other influences, the electrical parameters of these modules deviate from uniformity. Consequently, the amplitude-phase distribution of the electromagnetic field across the antenna aperture becomes non-uniform, resulting in a reduction in antenna gain and an increase in the side-lobe levels of the Radiation Pattern RP_{Σ} and Gain Patterns GP_{Σ}.

To ensure that the ICS operates with parameters aligned with theoretical calculations, it is essential to perform calibration not only at regular intervals but also in real time during operation. However, the calibration methods and techniques employed for these antenna arrays exhibit unique characteristics that differ markedly from those used for conventional antennas. This distinction is particularly relevant in the case of ICS where Digital Transceiver Modules (DTM) are synthesized using quadrature modulation and demodulation algorithms [2, 3]. This distinction arises from the process of synthesis and formation of the transmitting signal which is directly generated at each digital transceiver module. Unlike traditional active ICS, models, where the Radio Frequency (RF) transmitting signal is produced by a central source and distributed to system modules via a RF splitters and transmission cables, the ICS relies solely on digital data. This data encodes the parameters of the signal to be formed, eliminating the need for an intermediary RF splitters and transmission cables system. In conventional phased array antenna systems, the RF splitters and transmission cables itself introduces errors in the amplitude and phase of the RF signals at the input of the DTM [4–7]. By bypassing this system, the ICS architecture significantly reduces such errors.

The aforementioned factors can lead to imbalances between I and Q channels within the transmitting and receiving paths of DTM. To address these challenges, extensive research has focused on mitigating I/Q imbalances through diverse technical approaches. These studies commonly explore contributing factors, such as the operating frequency range of the radar sensor, the structural configuration of the receiving path, and the use of calibration signals. The ultimate goal is to develop and synthesize methods and models for automatic calibration using various approaches [8–15].

However, upon examining the aforementioned published results and other related studies, it can be seen that a small point has not been adequately addressed. Specifically, except for the external noise with high intensity, the power level of the reflected signals from the target objects of the ICS is often much smaller than the internal noise power level, as presented in [16, 17]. This characteristic necessitates careful consideration of power parameter synthesis for calibration signals. Moreover, the reliance on a rigidly synthesized reference object model may introduce additional errors in both measurement and automatic calibration processes. These observations form the foundation for the research presented in this paper.

Building on the preliminary analysis discussed above, the second section of this paper introduces a novel methodology for addressing the challenge of real-time automatic calibration of the receiving path in DTM of ICS grounded in the proposed mathematical model. This section also includes the synthesis of the structural diagram of the subsystem designed to implement this approach. The third section presents simulation and experimental results, demonstrating the correctness of the proposed methodology.

Theory and simulation of the proposed methodology

The novel methodology for solving the problem of real-time automatic calibration of the receiving path in DTM of ICS

According to [2, 3], the primary objective of the calibration process for any antenna system is to minimize the error between the measured gain pattern parameters and their theoretically calculated counterparts. The approach presented in this study for addressing the automatic calibration problem aligns with the overarching goal. Specifically, the formation of the calibration coefficients proposed here is based on the comparison of the receiving path output signal of each DTM with the receiving path output signal of the reference DTM using a calibration signal as the input. From a physical perspective, this method is not fundamentally novel. The novelty here is expressed as follows.

According to [2, 16, 17], the reflected signals received from targets via the antenna element and reaching the input of each receiving path are typically significantly weaker than the internal noise level, $P_{int.noise.}$, of the receiving path. Consequently, the design and implementation of a calibration signal must be carefully considered. An effective approach involves utilizing a RF calibration signal encoded with a Binary Phase-Shift Keying (BPSK), scheme featuring $M_{pos.}$ positions. The signal duration $t_{sig.}$ is designed to be $M_{pos.}$ times the width of an individual sub-pulse, $\tau_{sub.pul.}$ (Fig. 1). Furthermore, the power of the sub-pulse, $P_{\tau sub.pul.}$ at the input of the receiving path is deliberately adjusted to remain significantly lower than the $P_{int.noise.}$ of the receiving path to ensure accurate calibration. That is, the Signal-To-Noise Ratio (SNR) of the sub-pulse at the receiving path input $SNR_{sub.pul.}$ is within the limit (10^{-6}–10^{-3}) for the common radar operating frequency bands as presented in [18, 19].

Application of the approach Software-Defined Radio (SDR) technology utilizes a “virtual” reference DTM model. This model incorporates data on the input and output signal parameters for both the transmitting and receiving channels which are initially determined through theoretical calculations. These parameters are subsequently will be refined, supplemented, and calibrated using data obtained from the calibration process conducted at the manufacturing facility as well as during field deployment and operational phases. So, this approach effectively eliminates the potential errors of physical reference DTM during actual operation. To ensure accurate estimation of the calibration coefficient parameters for each receiving path, their output signals must be coherently accumulated with the required accumulation coefficient. For example, it is possible to accumulate according to $M_{pos.}$, or accumulate according to the number of receiving paths corresponding to the number $M_{col} \times N_{row}$ of DTM, in which, M_{col} and N_{row} are the column and row indices and columns of the ICS, respectively, where DTM are located at the intersection points of the row and column. The calibration value of the output complex signal amplitude for each DTM is determined by multiplying the output complex signal amplitude with the corresponding calibration coefficient. So, the GP_Σ of the ICS is synthesized by computing the weighted sum of the calibrated output complex signal amplitudes across the receiving channels. This process will ensure the largest possible value for the total gain pattern GP_Σ.

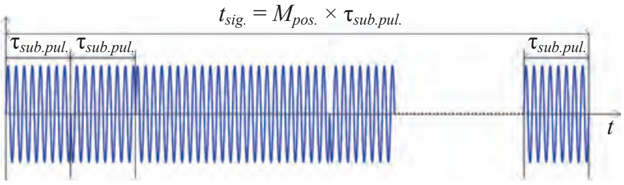

Fig. 1. The structure of the calibration signal

A mathematical model of the receiving paths during automatic calibration according to the proposed methodology

Consider an ICS comprising $M_{col} \times N_{row}$ DTM in which its architecture synthesized based on the principles of quadrature modulation and demodulation. The calibration signal $S(j\omega)$ is constructed using a BPSK code with $M_{pos.}$ positions [19, 20]. The use of a rectangular windowed Fourier transform is instrumental in the analysis of complex signal images. This signal consists of RF sub-pulses generated by a Controlled Signal Generator (CSG). The generated signal passes through a directional coupler element and is subsequently routed via a circulator element, functioning as a transceiver switch, to the input of the receiving path of the i-th DTM, where $i \in [1, M_{col} \times N_{row}]$ as illustrated in Fig. 2. In there, $i = 0$ represents the “virtual” reference DTM.

Consequently, to ensure the SNR reaches a sufficiently high level required for subsequent processing, the digital data will have to be coherently accumulated by required to

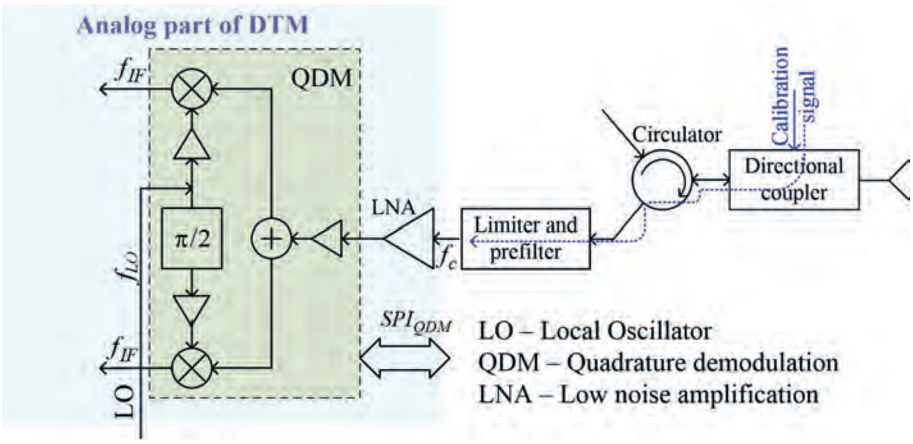

Fig. 2. The route of the calibration signal to the input of the receiving path: f_{IF} — intermediate frequency; f_{LO} — frequency of LO; SPI_{QDM} — serial peripheral interface of QDM; and f_c — carrier frequency

form a complex signal $S_i(j\omega)$. This signal comprises two components, real and imaginary, structured in the form:

$$\mathrm{Re}S_i(j\omega) = \sum_m^M \mathrm{Re}S_{m.i}(j\omega);\ \mathrm{Im}S_i(j\omega) = \sum_m^M \mathrm{Im}S_{m.i}(j\omega), \quad (1)$$

where, M is the number of coherent accumulations, and $m = 1, 2, \ldots, M$. If we consider $M \cong M_{pos.}$, the process of coherent accumulation can be interpreted as the sub-pulses being accumulated in accordance with M_{pos}. Furthermore, additionally coherent accumulation with $M_{col} \times N_{row}$, the expression (1) will be in the form:

$$\mathrm{Re}S_i(j\omega) = \sum_p^{M_{col}\times N_{row}} \sum_m^{M_{pos.}} \mathrm{Re}S_{p.m.i}(j\omega);$$

$$\mathrm{Im}S_i(j\omega) = \sum_p^{M_{col}\times N_{row}} \sum_m^{M_{pos.}} \mathrm{Im}S_{p.m.i}(j\omega).$$

From this point, the complex calibration coefficient can be defined for each i-th receiving path:

$$K_i(j\omega) = \frac{S_0(j\omega)}{S_i(j\omega)} = \frac{|S_0(j\omega)|\times\exp(j\varphi_0)}{|S_i(j\omega)|\times\exp(j\varphi_i)}. \quad (2)$$

Where $|S_0(j\omega)|$ and φ_0 denote the amplitude and phase, respectively, of the accumulated complex signal corresponding to the receiving path of the reference module. And $|S_i(j\omega)|$ and $|\varphi_i|$ represent the amplitude and phase, respectively, of the accumulated complex signal associated with the receiving path of the i-th module undergoing calibration. The values of $|S_{\Sigma.i}(j\omega)|$ and φ_i are determined by the expression: $|S_i(j\omega)| = \sqrt{(\mathrm{Re}S_i(j\omega))^2 + (\mathrm{Im}S_i(j\omega))^2}$; $\varphi_i = \mathrm{arctg}(\mathrm{Im}S_i(j\omega))/\mathrm{Re}S_i(j\omega)$.

During the process of coherent accumulation, whether following $M_{pos.}$ or using $M_{col} \times N_{row}$, the absolute value of the complex amplitude $|S_{\Sigma.0}(j\omega)|$ for the reference channel and $|S_{\Sigma.i}(j\omega)|$ for the channel undergoing calibration can be expressed in the following form: $|S_{\Sigma.0}(j\omega)| = M_{pos.} \times |S_i(j\omega)|$ or $|S_{\Sigma.0}(j\omega)| = M_{pos.}(M_{col} \times N_{row}) \times |S_0(j\omega)|$; $|S_{\Sigma.i}(j\omega)| = M_{pos.} \times |S_i(j\omega)|$ or $|S_{\Sigma.i}(j\omega)| = M_{pos.}(M_{col} \times N_{row}) \times |S_i(j\omega)|$.

The complex calibration coefficient for each receiving path in expression (2) can be rewritten as $K_i(j\omega) = |K_i(j\omega)|\exp(j\Delta\varphi_i)$.

Where, $|K_i(j\omega)|$ is defined as the absolute value of the complex calibration coefficient for the i-th receiving path, and the $\Delta\varphi_i = \varphi_0 - \varphi_i$ represents the magnitude of the phase error that requires correction. It is possible to write that: $|K_i(j\omega)| = |S_0(j\omega)|/|S_i(j\omega)|$. This equation is expressed in the form of a trigonometric function: $K_i(j\omega) = |K_i(j\omega)| \times [\cos(\Delta\varphi_i) + j\sin(\Delta\varphi_i)]$. And, with two real and imaginary parts: $\mathrm{Re}K_i(j\omega) = |K_i(j\omega)| \times \cos(\Delta\varphi_i)$; $\mathrm{Im}\,K_i(j\omega) = |K_i(j\omega)|\times\sin(\Delta\varphi_i)$.

The complex amplitude of the signal at the output of the receiving path, $S_{out.i}(j\omega)$, expressed in both exponential and trigonometric forms, is represented as follows: $S_{out.i}(j\omega) = |S_{out.i}(j\omega)| \times \exp(j\varphi_i)$; $S_{out.i}(j\omega) = |S_{out.i}(j\omega)| \times [\cos(\varphi_i) + j\sin(\varphi_i)]$.

The product of the complex amplitude of the output signal from the i-th receiving path and the corresponding complex calibration coefficient for that path can be represented in the following form: $S_{out.i}(j\omega) \times K_i(j\omega) = |S_{out.i}(j\omega)| \times |K_i(j\omega)|[\cos(\varphi_i + \Delta\varphi_i) + j\sin(\varphi_i + \Delta\varphi_i)]$. We have: $|S_{out.0}(j\omega)| = |S_0(j\omega)|$; $|S_{out.i}(j\omega)| = |S_i(j\omega)|$, and $S_{out.i}(j\omega) \times K_i(j\omega) = |S_0(j\omega)| \times [\cos(\varphi_0) + j\sin(\varphi_0)]$. This equation represents the calibrated complex amplitude of the input signal for the i-th receiving path. And, it can also be expressed either in exponential form or as two separate components, namely, the real and imaginary parts, as follows:

$$S_{i\,cal.}(j\omega) = |S_0(j\omega)| \times \exp(j\varphi_0)$$
$$\text{and } \mathrm{Re}S_{i\,cal.}(j\omega) = |S_0(j\omega)| \times \cos(\varphi_0);$$
$$\mathrm{Im}S_{i\,cal.}(j\omega) = |S_0(j\omega)| \times j\sin(\varphi_0).$$

These components are precisely equal to the quadrature components of the complex amplitude of the output signal from the reference receiving path. Thus, after calibration, the output signals of all paths will be identical in both amplitude and phase.

Synthesis of the subsystem diagram for real-time automatic calibration of the receiving path in DTM of the ICS

Based on the results derived from the proposed mathematical model, the process for automatic calibration of the receiving path in the DTM can be synthesized with the following key considerations:

— Calibration Signal Timing: The calibration signal is supplied in to the input of the receiving path during the time interval corresponding to the receiving period of the radar sensor reflected signals (Fig. 3).

— Signal Blocking: To minimize errors caused by interference, the calibration signal is isolated by a detection unit that filters out reflected signals and significant external noise (Fig. 4).

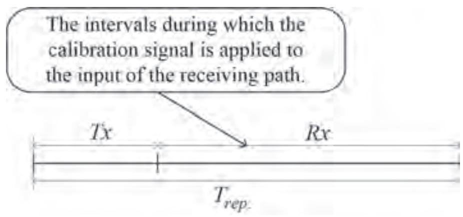

Fig. 3. The receiving period *Rx*: *Tx* is the transmission interval of the signal.
$T_{rep.}$ — period repeats

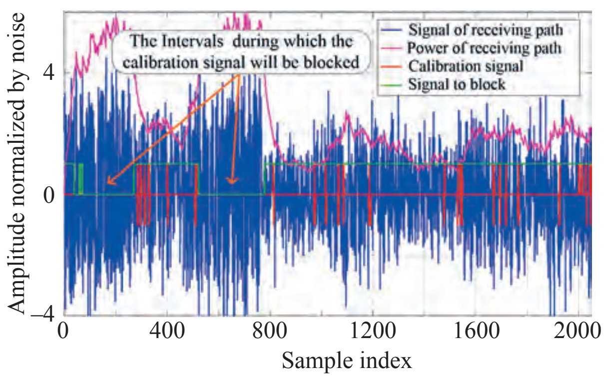

Fig. 4. The intervals during which the calibration signal will be blocked

— “Virtual” reference DTM structure: The “virtual” reference DTM consists of two primary components: the first component is integrated within the Central Computing and Processing Unit (CCPU), and generates control data containing information about the structure of $S_0(j\omega)$. The second component is a CSG which is structurally independent and operates in isolation within the digital part of the transmitting part in the DTM to form $S_0(j\omega)$.

Fig. 5 presents the structural diagram of the automatic calibration subsystem for the receiving path within the DTM of the ICS. Accordingly, in each DTM, the calibration signal is generated by the CSG based on input data provided by the CCPU which includes information regarding the formation of the signal and periodic updates. The CSG produces the calibration signal $S_i(j\omega)$, with parameters $t_{sig.}$, $\tau_{sub.pul.}$ and $P_{\tau sub.pul.} << P_{int.noise.}$, which is transmitted to the receiving paths upon receiving the P_x command. An instantaneous power meter monitors the power level of the received signal which includes both reflected signals and external noise. If the measured power level significantly exceeds the internal noise power, the blocking command will be formed and sent to the CCPU, enabling it to bloke the supply of calibration signal data for each CSG.

Following single-pulse filtering, the output of the each i-th DTM produces two quadrature components of the calibration signal, $\mathrm{Re}S_i(j\omega)$ and $\mathrm{Im}S_i(j\omega)$. These components are transmitted to the Calculation and Automatic Calibration Unit (C&ACU) where accumulation operations, specifically digital coherent accumulation processing, are performed based on the indices $M_{pos.}$, or $M_{pos.}$ and $M_{col} \times N_{row}$, as required. Subsequently, the processed data are compared with the corresponding data of the reference signal to estimate the calibration coefficients $K_i(j\omega)$ and to form the data of $S_{i.n.}(j\omega)$, for generating the necessary $S_i(j\omega)$. Data of $S_{i.n.}(j\omega)$ is transmitted to the CSG_i of the i-th DTM according to the specified address, and forwarded to the CCPU. Additionally, the digital data of $\mathrm{Re}S_{i\ cal.}(j\omega)$ and $\mathrm{Im}S_{i\ cal.}(j\omega)$ with $i \in (M_{col} \times N_{row})$ are transmitted to the GP_Σ formation unit.

It is easy to see that the functional units involved in the real-time automatic calibration of the receiving path within the DTM are integral components of both the basic architecture of the DTM and the overall ICS. Notably, the calibration process necessitates only a minimal addition of hardware components. Consequently, the use of the term “integrated subsystem” to explain in this study is entirely justified.

Simulation of the proposed methodology

The simulation conducted to validate the theoretical research findings incorporates the components illustrated in Fig. 6. These include four receiving paths where structural improvements aimed at adaptive dynamic range control have been implemented as described in [17]; a Local Oscillator voltage generation and Distribution Unit (LO&DU); an Automatic Calculation, Calibration, and Control Unit (CAC&CU); and a computer serving as the central processing and display interface. The signal parameters utilized during the simulation are: f_0 = 1560–1590 MHz; f_{LO} = 1470–1500 MHz; f_{IF} = 90 MHz; $M_{pos.}$ = 256. Fig. 7 presents the simulation results of signals from the four receiver paths ($M_{rec.p.}$ = 4), both prior to and following the automatic calibration process.

The cumulative processing is conducted with $M = M_{pos.} \times M_{rec.p.} = 256 \times 4 = 1024$, corresponding to the number of samples. For the sake of simplifying the simulation process, it is assumed that the receiving path No 1 serves as the reference path. Table 1 present the results

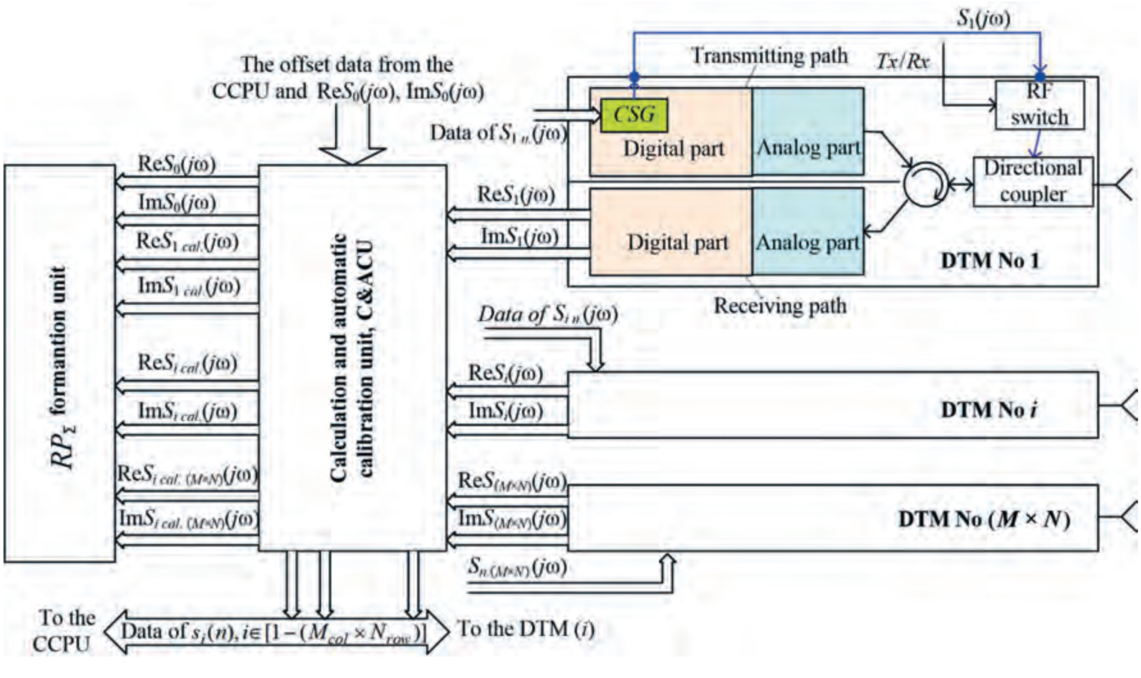

Fig. 5. The general structural diagram of the automatic calibration subsystem for the receiving path within the DTM of the ICS: RP_Σ — Radiation Pattern after beamforming; S_{1cal} — the first calibration signal; $S_{i\ cal}$ — the i-th calibration signal; $S_{i\ cal(M\times N)}$ — the i-th calibration signal at M_{col} and N_{row}; $S_{1\ n.}$ — the reference of the first signal; $S_{i\ n.}$ — the reference of the i-th signal; $S_i(M\times N)$ — the reference of the i-th signal at M_{col} and N_{row}

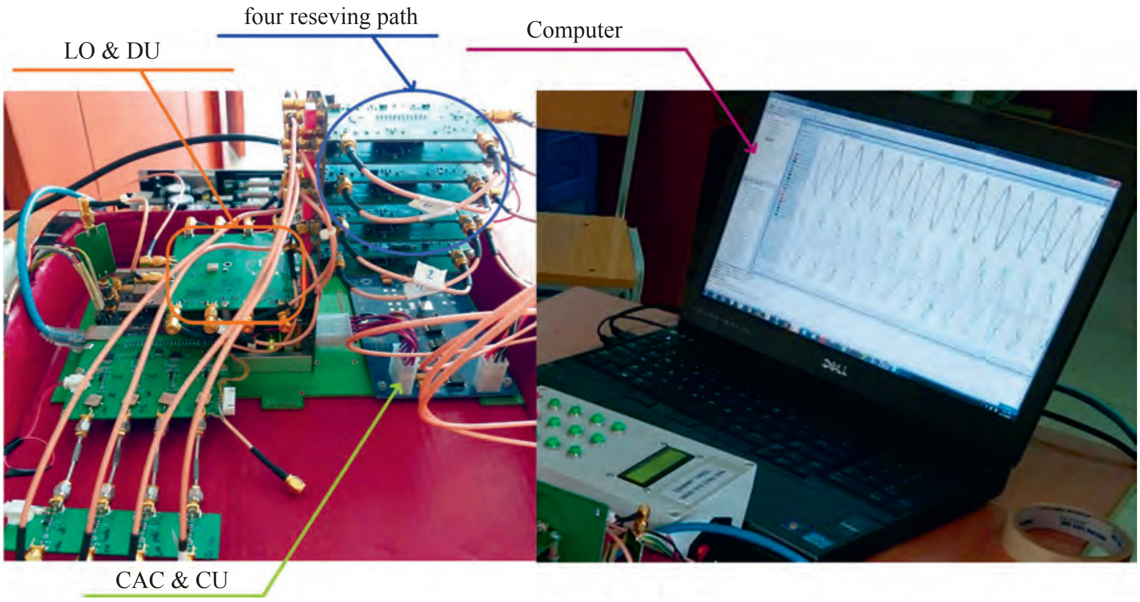

Fig. 6. Diagram illustrating the implementation of the simulation for the subsystem responsible for the automatic calibration of receiving paths (four paths)

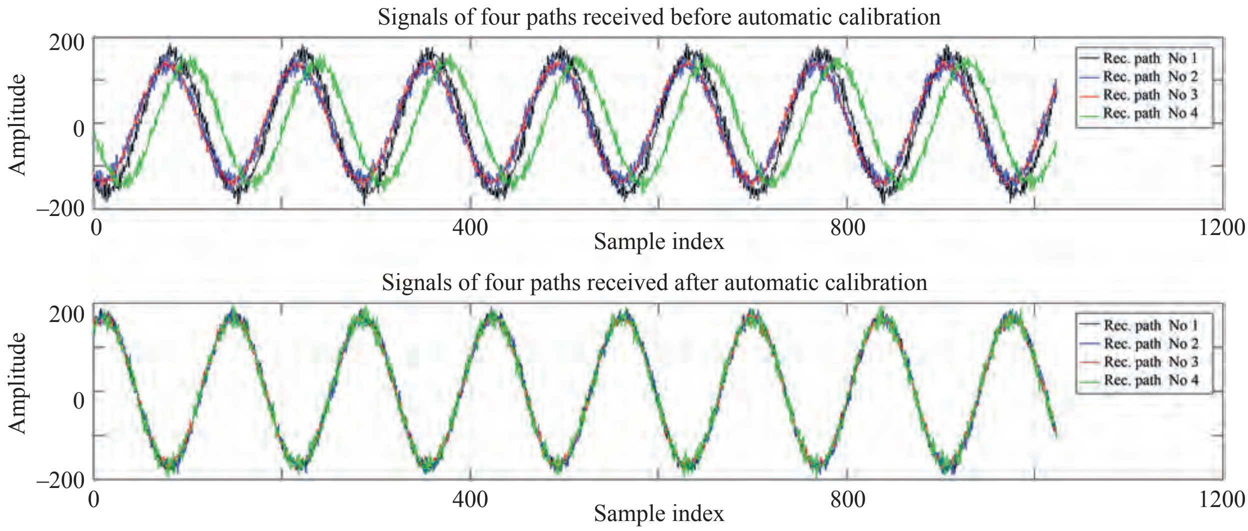

Fig. 7. Simulation results of signals from the four receiver paths, both prior to and following the automatic calibration process

Table 1. Values of the signal amplitude and phase errors, without incorporating improvements to the receiving path model

State of the receiving path	Path No 2	Path No 3	Path No 4
Signal amplitude error (*), dB			
Before calibration	2.20	1.90	2.60
After calibration	0.25	0.34	0.41
Signal phase error (*)			
Before calibration	6°18′	5°30′	7°12′
After calibration	1°36′	2°00′	1°06′

Note. (*) Compared to the reference receiving path.

of the estimation of amplitude and phase errors of the signal, both before and after calibration. These estimations were performed without incorporating improvements to the receiving path model, which was synthesized as a model of a fully matched filter, and without implementing adaptive dynamic range control.

Table 2 presents the results of the estimation of amplitude and phase errors of the signal, both before and

Table 2. Values of the signal amplitude and phase errors, when incorporating improvements to the receiving path model

State of the receiving path	Path No 2	Path No 3	Path No 4
Signal amplitude error (*), dB			
Before calibration	3.10	2.30	2.80
After calibration	0.14	0.13	0.16
Signal phase error (*)			
Before calibration	4°30′	6°18′	7°12′
After calibration	0°48′	1°06′	0°42′

Note. (*) Compared to the reference receiving path.

after calibration. These estimations were performed when incorporating improvements to the receiving path model which was synthesized as a model of a fully matched filter, and with implementing adaptive dynamic range control.

The methodology for identifying amplitude and phase errors is comprehensively described in [18, 19, 21]. The simulation results validate the correctness of the proposed methodology. Specifically, as presented in Table 1, the magnitude of amplitude errors is reduced, ranging from 1.95 dB to 2.19 dB and phase errors decrease to values between 3°30′ and 6°06′. Furthermore, implementing the solutions to enhance the receiving path yields further reductions in error magnitudes, for both the amplitude and phase of the signal. This improvement significantly enhances the formation of GP_Σ as evidenced by parameters such as peak gain and the suppression of the sub-lobes, as illustrated in Fig. 9.

Results and Discussion

The validity of the proposed methodology is further corroborated through experimental verification. The experimental setup is depicted in Fig. 8 and consists of a radar sensor system equipped with four receiving paths, each comprising a DTM connected to an individual antenna element (Fig. 8, *a*), all mounted on a turntable (Fig. 8, *c*). Additionally, the system includes a CSG and its associated irradiation antenna (Fig. 8, *b*), positioned at a specified distance D from the radar probe system to ensure the incident waves can be approximated as plane waves. A computer serves as the CCPU and display. The catalogue of key components employed in the experiment is presented in Table 3.

For a frequency f_0 in the range of 1560–1590 MHz, the far-field region is considered to be at distances greater than 2 m. The experiment was conducted with a separation r of 7.5 m between the radiation antenna and the antenna system of ICS. To consistent with the simulation procedure, the experiment utilized the first receiving path as the reference path.

The experimental results, summarized in Tables 4, and 5, present the errors in signal amplitude and phase both before and after calibration. Additionally, the results also illustrate the effects of enhancements to the receiving path, implemented based on the fully matched filter model and the dynamic range adaptive control methodology.

Experimental results were also obtained by synthesizing GP_Σ for different observation angles, utilizing a turntable to rotate the ICS. These results were compared with those generated through simulation after calibration. Fig. 9 presents the synthesized GP_Σ obtained via the simulation method post-calibration. Fig. 10 illustrates the results derived from measuring and processing the experimental data.

Both GP_Σ synthesis results were obtained under conditions in which the receiving paths were improved

Table 3. Catalogue of the key components used in the experiment

Brands	Part Number	Applications
Macom	CG2H40010	Power amplifier
Macom	CMPA0527005	Power preamplifier
MAX	MAX2021	Direct Up/Down conversion Quadrature Mod/Demod
MAX	MAX9491 or equivalent	VCO and Synth
TI	DAC3283 or equivalent	16-Bits DAC
TI	ADC3683 or equivalent	High-speed ADCs
UMS	CHA3801-99F	L-Band LNA
UMS	GVA-63+	IF Amplifier
AD	ADL5531 or equivalent	Voltage-controlled amplifier/attenuator Operating frequency
AD	AD9914S or equivalent	3.5 GSPS Direct Digital Synthesizer with 12-Bit DAC
AD	AD9833 EP	CSG (Programmable Waveform Generator)
Atmel	AVR2560/V	8-Bit Atmel Microcontroller with

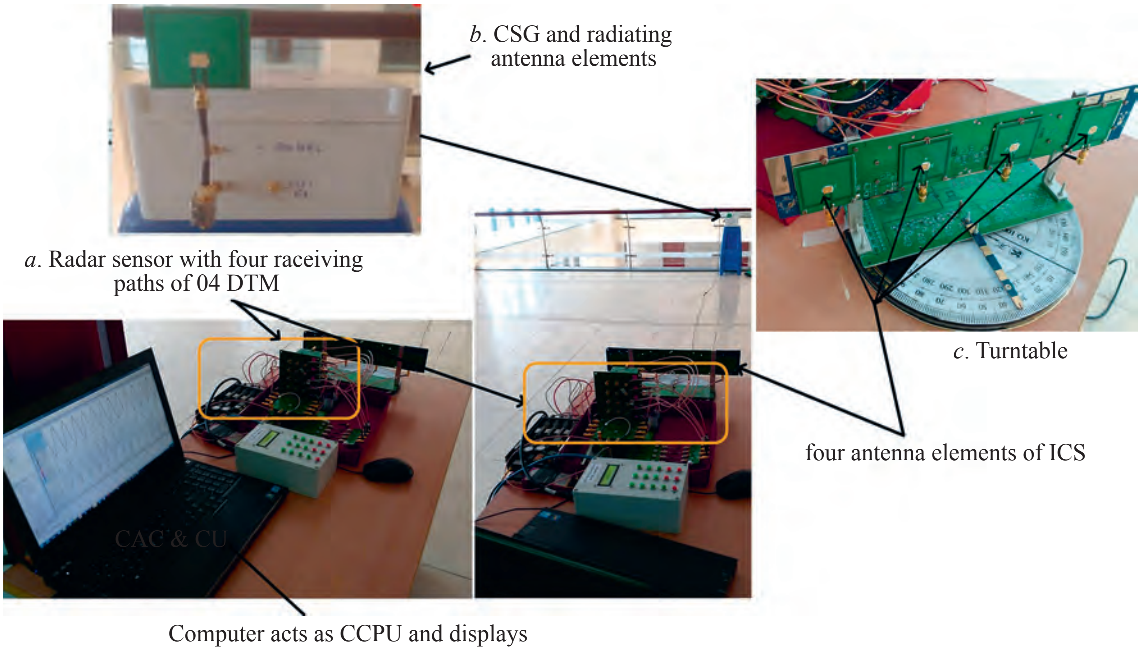

Fig. 8. Experimental setup for validating the proposed methodology

Table 4. Experimental results determine the signal amplitude and phase errors before improving the receiving path

State of the receiving path	Path No 2	Path No 3	Path No 4
Signal amplitude error (*), dB			
Before calibration	5.50	6.30	7.10
After calibration	0.91	1.34	1.53
Signal phase error (*)			
Before calibration	8°06′	9°06′	6°54′
After calibration	2°12′	2°42′	1°48′

Note. (*) Compared to the reference receiving path.

Table 5. Experimental results determine the signal amplitude and phase errors after improving the receiving path

State of the receiving path	Path No 2	Path No 3	Path No 4
Signal amplitude error (*), dB			
Before calibration	6.10	6.30	5.50
After calibration	0.41	0.34	0.25
Signal phase error (*)			
Before calibration	7°36′00″	6°48′00″	7°18′00″
After calibration	0°14′24″	0°12′36″	0°18′36″

Note. (*) Compared to the reference receiving path.

through the application of a fully matched filter model and dynamic range adaptive control. Based on the simulation and experimental results presented above, several observations can be made as follows:

— The proposed methodology for automatic measurement and calibration of the receiving paths in DTM has been validated both theoretically and experimentally. While experimental data exhibit some phase and amplitude errors compared to theoretical calculations and simulations; these discrepancies can be attributed to factors, such as coefficient estimation errors, quantization noise, and hardware and software imperfections. These findings provide valuable insights for further improvement in research, design, and production processes.
— Accurate determination of errors in the calculation and establishment of calibration coefficients can be achieved through adaptive adjustments to the number of coherent accumulations across all receiving paths, as outlined in this study.
— In principle, the calibration process model can be characterized as “automatic, real-time, and integrated”.

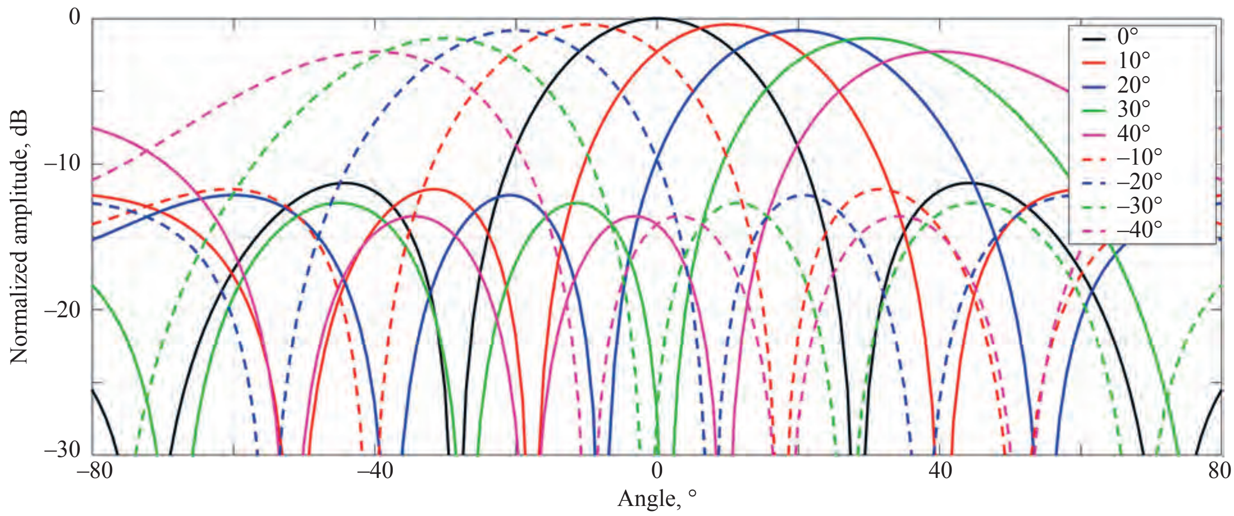

Fig. 9. The GP_Σ obtained through simulation after calibration

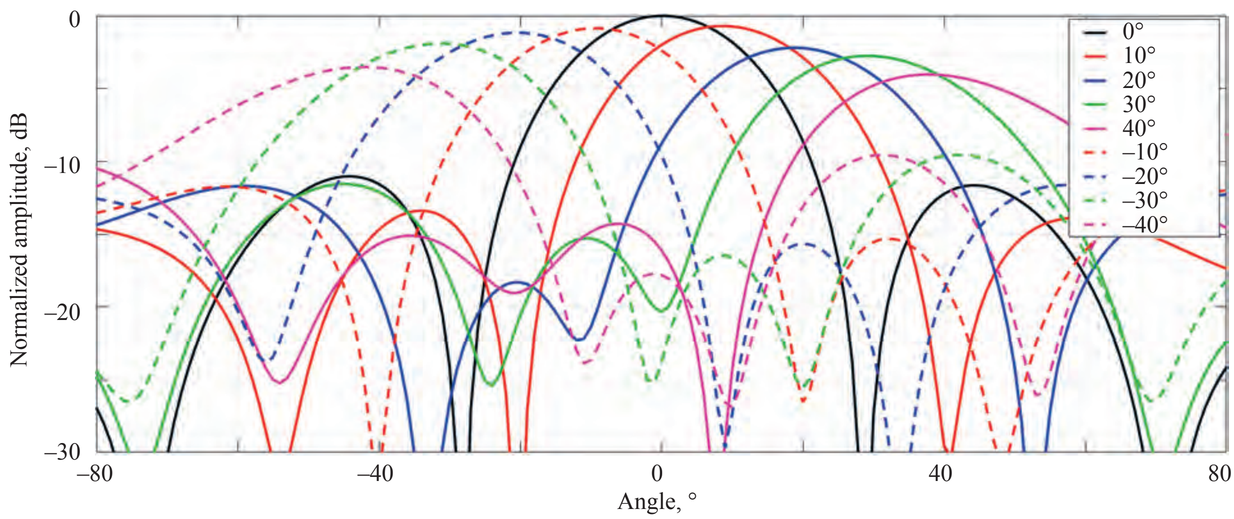

Fig. 10. The GP_Σ is synthesized after calibration and according to the measurement data: the GP_Σ are synthesized at angles: 0°, ±10°, ±20°, ±30° and ±40°

This is because the measurement and estimation of errors are conducted entirely automatically and concurrently with the system operational processes. Furthermore, the hardware and software components are seamlessly integrated and implemented within the essential elements required for ICS in general and for each DTM specifically.

Conclusions

The primary focus of the paper is to propose a novel methodology for real-time automatic calibration of the Information and Control System (ICS), specifically targeting the receiving path in the Digital Transceiver Module (DTM). The innovation of this approach stems from leveraging the difference in power levels of reflected signals observed at the receiver input of a radar sensor using a conventional antenna and the input of the receiving path in the DTM of the ICS. To achieve accurate calibration, it is critical to ensure that the power level of the calibration signal aligns with the minimal power level of the reflected signal. Accurate estimation of amplitude and phase errors in the calibration signal as it propagates through the receiving path requires coherent accumulation using appropriate accumulation coefficients. This process enhances precision in error quantification. The methodology introduces a virtual reference DTM model, synthesized using a “soft configuration” approach, to serve as a reference receiving path. This virtual model effectively replaces the physical reference DTM, mitigating potential errors that could arise during operation. Calibration coefficients are derived by comparing the complex signal amplitude of the receiving path in the virtual reference DTM with the complex signal amplitudes of other receiving paths after coherent accumulation. The calibration values for each module output are computed by multiplying the complex signal amplitude by the corresponding calibration coefficient. The synthesis for the gain patterns of the ICS are weighted summation of the calibrated complex signal amplitudes of the receiving paths. This synthesis ensures optimal performance by maximizing peak gain and minimizing side lobe levels in the system.

References

1. Kedar A. Phased array antenna for radar application. *Handbook of Metrology and Applications*, 2023, pp. 1443–1469. https://doi.org/10.1007/978-981-99-2074-7_81
2. Ttofis C., Papadopoulos A., Theocharides T., Michael M.K., Doumenis D. An MPSoC-based QAM modulation architecture with run-time load-balancing. *Eurasip Journal on Embedded Systems*, 2011, no. 1, pp. 790265. https://doi.org/10.1155/2011/790265
3. Fischer W. Basic principles of digital modulation. *Signals and Communication Technology*, 2010, no. 3 rd, pp. 219–260. https://doi.org/10.1007/978-3-642-11612-4_13
4. Lu Guoming, Zakharov P.N., Korolev A.F. Digital phased antenna array transceiver with multibeam radiation pattern. *Bulletin of the Russian Academy of Sciences: Physics*, 2023, vol. 87, no. 1, pp. 51–54. https://doi.org/10.3103/S1062873822700125
5. Babur G., Manokhin G.O., Monastyrev E.A., Geltser A.A., Shibelgut A.A. Simple calibration technique for phased array radar systems. *Progress in Electromagnetics Research M*, 2017, vol. 55, pp. 109–119. https://doi.org/10.2528/PIERM16101203
6. Agrawal A., Jablon A. A calibration technique for active phased array antennas. *Proc. of the IEEE International Symposium on Phased Array Systems and Technology*, 2003, pp. 223–228. https://doi.org/10.1109/PAST.2003.1256985
7. Pan C., Ba X., Tang Y., Zhang F., Zhang Y., Wang Z., Fan W. Phased array antenna calibration method experimental validation and comparison. *Electronics*, 2023, vol. 12, no. 3, pp. 489. https://doi.org/10.3390/electronics12030489
8. Wang R., Gao P., Liu J., Wang Z., Wang C., Yu F. A hybrid scheme for TX I/Q imbalance self-calibration in a direct-conversion transceiver. *Electronics*, 2024, vol. 13, no. 9, pp. 1653. https://doi.org/10.3390/electronics13091653
9. Peng X., Wang Z., Mo J., Wang C., Liu J., Yu F. A blind calibration model for I/Q imbalances of wideband zero-IF receivers. *Electronics*, 2020, vol. 9, no. 11, pp. 1868. https://doi.org/10.3390/electronics9111868
10. Djigan V.I., Kurganov V.V. Antenna array calibration algorithm without access to channel signals. *Radioelectronics and Communications Systems*, 2020, vol. 63, no. 1, pp. 1–14. https://doi.org/10.3103/S073527272001001X
11. Lim A.G.K.C., Sreeram V., Wang G.-Q. Digital compensation in IQ modulators using adaptive FIR filters. *IEEE Transactions on Vehicular Technology*, 2004, vol. 53, no. 6, pp. 1809–1817. https://doi.org/10.1109/TVT.2004.836934
12. Tuthill J., Cantoni A. Efficient compensation for frequency-dependent errors in analog reconstruction filters used in IQ modulators. *IEEE Transactions on Communications*, 2005, vol. 53, no. 3, pp. 489–496. https://doi.org/10.1109/tcomm.2005.843455
13. He G., Gao X., Zhang R. Impact analysis and calibration methods of excitation errors for phased array antennas. *IEEE Access*, 2021, vol. 9, pp. 59010–59026. https://doi.org/10.1109/ACCESS.2021.3073222
14. Anttila L., Valkama M., Renfors M. Circularity-Based I/Q imbalance compensation in wideband direct-conversion receivers. *IEEE Transactions on Vehicular Technology*, 2008, vol. 57, no. 4, pp. 2099–2113. https://doi.org/10.1109/TVT.2007.909269
15. Li H., Liu A., Yang Q., Yu C., Lyv Z. Antenna pattern calibration method for phased array of high-frequency surface wave radar based on first-order sea clutter. *Remote Sensing*, 2023, vol. 15, no. 24, pp. 5789. https://doi.org/10.3390/rs15245789
16. Viet H.T., Minh T.H. A real-time internal calibration method for radar systems using digital phase array antennas. *Lecture Notes of the Institute for Computer Sciences, Social-Informatics and Telecommunications Engineering*, 2021, vol. 379, pp. 88–103. https://doi.org/10.1007/978-3-030-77424-0_8
17. Nguyen X.L., Thi T.T.D., Nguyen P.B., Tran V.H. Receiving paths improvement of digital phased array antennas using adaptive dynamic range. *Electronics*, 2024, vol. 13, no. 21, pp. 4161. https://doi.org/10.3390/electronics13214161
18. Peter D. Hybrid beamforming receiver dynamic range theory to practice. *Microwave Product Digest & Technologies*. 2022.
19. Chen Y., Ming C., Xie K., Gao S., Jiang Q., Liu Z., Yao H., Dong K. All-in-One BPSK/QPSK switchable transmission and reception for adaptive free-space optical communication links. *Photonics*, 2024, vol. 11, no. 4, pp. 326. https://doi.org/10.3390/photonics11040326
20. Qi C., Wu L. PLL demodulation technique for M-ray Position Phase Shift Keying. *Journal of Electronics (China)*, 2009, vol. 26, no. 3, pp. 289–295. https://doi.org/10.1007/s11767-008-0021-z

Литература

1. Kedar A. Phased array antenna for radar application // Handbook of Metrology and Applications. 2023. P. 1443–1469. https://doi.org/10.1007/978-981-99-2074-7_81
2. Ttofis C., Papadopoulos A., Theocharides T., Michael M.K., Doumenis D. An MPSoC-based QAM modulation architecture with run-time load-balancing // Eurasip Journal on Embedded Systems. 2011. N 1. P. 790265. https://doi.org/10.1155/2011/790265
3. Fischer W. Basic principles of digital modulation // Signals and Communication Technology. 2010. N 3 rd. P. 219–260. https://doi.org/10.1007/978-3-642-11612-4_13
4. Lu Guoming, Zakharov P.N., Korolev A.F. Digital phased antenna array transceiver with multibeam radiation pattern // Bulletin of the Russian Academy of Sciences: Physics. 2023. V. 87. N 1. P. 51–54. https://doi.org/10.3103/S1062873822700125
5. Babur G., Manokhin G.O., Monastyrev E.A., Geltser A.A., Shibelgut A.A. Simple calibration technique for phased array radar systems // Progress in Electromagnetics Research M. 2017. V. 55. P. 109–119. https://doi.org/10.2528/PIERM16101203
6. Agrawal A., Jablon A. A calibration technique for active phased array antennas // Proc. of the IEEE International Symposium on Phased Array Systems and Technology. 2003. P. 223–228. https://doi.org/10.1109/PAST.2003.1256985
7. Pan C., Ba X., Tang Y., Zhang F., Zhang Y., Wang Z., Fan W. Phased array antenna calibration method experimental validation and comparison // Electronics. 2023. V. 12. N 3. P. 489. https://doi.org/10.3390/electronics12030489
8. Wang R., Gao P., Liu J., Wang Z., Wang C., Yu F. A hybrid scheme for TX I/Q imbalance self-calibration in a direct-conversion transceiver // Electronics. 2024. V. 13. N 9. P. 1653. https://doi.org/10.3390/electronics13091653
9. Peng X., Wang Z., Mo J., Wang C., Liu J., Yu F. A blind calibration model for I/Q imbalances of wideband zero-IF receivers // Electronics. 2020. V. 9. N 11. P. 1868. https://doi.org/10.3390/electronics9111868
10. Djigan V.I., Kurganov V.V. Antenna array calibration algorithm without access to channel signals // Radioelectronics and Communications Systems. 2020. V. 63. N 1. P. 1–14. https://doi.org/10.3103/S073527272001001X
11. Lim A.G.K.C., Sreeram V., Wang G.-Q. Digital compensation in IQ modulators using adaptive FIR filters // IEEE Transactions on Vehicular Technology. 2004. V. 53. N 6. P. 1809–1817. https://doi.org/10.1109/TVT.2004.836934
12. Tuthill J., Cantoni A. Efficient compensation for frequency-dependent errors in analog reconstruction filters used in IQ modulators // IEEE Transactions on Communications. 2005. V. 53. N 3. P. 489–496. https://doi.org/10.1109/tcomm.2005.843455
13. He G., Gao X., Zhang R. Impact analysis and calibration methods of excitation errors for phased array antennas // IEEE Access. 2021. V. 9. P. 59010–59026. https://doi.org/10.1109/ACCESS.2021.3073222
14. Anttila L., Valkama M., Renfors M. Circularity-Based I/Q imbalance compensation in wideband direct-conversion receivers // IEEE Transactions on Vehicular Technology. 2008. V. 57. N 4. P. 2099–2113. https://doi.org/10.1109/TVT.2007.909269
15. Li H., Liu A., Yang Q., Yu C., Lyv Z. Antenna pattern calibration method for phased array of high-frequency surface wave radar based on first-order sea clutter // Remote Sensing. 2023. V. 15. N 24. P. 5789. https://doi.org/10.3390/rs15245789
16. Viet H.T., Minh T.H. A real-time internal calibration method for radar systems using digital phase array antennas // Lecture Notes of the Institute for Computer Sciences, Social-Informatics and Telecommunications Engineering. 2021. V. 379. P. 88–103. https://doi.org/10.1007/978-3-030-77424-0_8
17. Nguyen X.L., Thi T.T.D., Nguyen P.B., Tran V.H. Receiving paths improvement of digital phased array antennas using adaptive dynamic range // Electronics. 2024. V. 13. N 21. P. 4161. https://doi.org/10.3390/electronics13214161
18. Peter D. Hybrid beamforming receiver dynamic range theory to practice // Microwave Product Digest & Technologies. 2022.
19. Chen Y., Ming C., Xie K., Gao S., Jiang Q., Liu Z., Yao H., Dong K. All-in-One BPSK/QPSK switchable transmission and reception for adaptive free-space optical communication links // Photonics. 2024. V. 11. N 4. P. 326. https://doi.org/10.3390/photonics11040326
20. Qi C., Wu L. PLL demodulation technique for M-ray Position Phase Shift Keying // Journal of Electronics (China). 2009. V. 26. N 3. P. 289–295. https://doi.org/10.1007/s11767-008-0021-z

21. Duong V.M., Vesely J., Hubacek P., Janu P., Phan N.G. Detection and parameter estimation analysis of binary shift keying signals in high noise environments. *Sensors*, 2022, vol. 22, no. 9, pp. 3203. https://doi.org/10.3390/s22093203

Authors

Nguyen Trong Nhan — PhD, Researcher, Air Defense - Air Force Technical Institute, Hanoi, 11400, Vietnam, sc 57222239467, https://orcid.org/0000-0001-6626-893X, 10th20th30th@gmail.com

Xuan Luong Nguyen — PhD Student, VNU University of Science, Hanoi, 100000, Vietnam, https://orcid.org/0009-0000-6988-4738, nguyenxuanluong_sdh22@hus.edu.vn

Phung Bao Nguyen — PhD, Associate Professor, Le Quy Don Technical University, Hanoi, 11917, Vietnam nguyenphungbao@lqdtu.edu.vn

Received 22.01.2025
Approved after reviewing 07.03.2025
Accepted 24.05.2025

21. Duong V.M., Vesely J., Hubacek P., Janu P., Phan N.G. Detection and parameter estimation analysis of binary shift keying signals in high noise environments // Sensors. 2022. V. 22. N 9. P. 3203. https://doi.org/10.3390/s22093203

Авторы

Нхан Нгуен Чонг — кандидат технических наук, исследователь, Технический институт ПВО, Ханой, 11400, Вьетнам, sc 57222239467, https://orcid.org/0000-0001-6626-893X, 10th20th30th@gmail.com

Нгуен Суан Лыонг — аспирант, Ханойский государственный университет, Ханой, 100000, Вьетнам, https://orcid.org/0009-0000-6988-4738, nguyenxuanluong_sdh22@hus.edu.vn

Нгуен Фунг Бао — кандидат технических наук, доцент, преподаватель, Вьетнамский государственный технический университет имени Ле Куй Дона, Ханой, 11917, Вьетнам, nguyenphungbao@lqdtu.edu.vn

Статья поступила в редакцию 22.01.2025
Одобрена после рецензирования 07.03.2025
Принята к печати 24.05.2025